

## Efficient single photon emission from a high-purity hexagonal boron nitride crystal

L. J. Martínez,<sup>1</sup> T. Pelini,<sup>1</sup> V. Waselowski,<sup>2</sup> J. R. Maze,<sup>2</sup> B. Gil,<sup>1</sup> G. Cassabois,<sup>1</sup> and V. Jacques<sup>1,\*</sup>

<sup>1</sup>Laboratoire Charles Coulomb, Université de Montpellier and CNRS, 34095 Montpellier, France

<sup>2</sup>Facultad de Física, Pontificia Universidad Católica de Chile, Santiago 7820436, Chile

(Received 15 June 2016; published 22 September 2016)

Among a variety of layered materials used as building blocks in van der Waals heterostructures, hexagonal boron nitride (hBN) appears as an ideal platform for hosting optically active defects owing to its large band gap ( $\sim 6$  eV). Here we study the optical response of a high-purity hBN crystal under green laser illumination. By means of photon correlation measurements, we identify individual defects emitting a highly photostable fluorescence under ambient conditions. A detailed analysis of the photophysical properties reveals a high quantum efficiency of the radiative transition, leading to a single photon source with very high brightness ( $\sim 4 \times 10^6$  counts  $s^{-1}$ ). These results illustrate how the wide range of applications offered by hBN could be further extended to photonic-based quantum information science and metrology.

DOI: [10.1103/PhysRevB.94.121405](https://doi.org/10.1103/PhysRevB.94.121405)

Hexagonal boron nitride (hBN), also known as “white graphite,” is a wide-band-gap material which has been commonly used in the industry for several decades owing to its high thermal and chemical stability [1,2]. Continuous improvement of growth techniques has recently enabled one to decrease the density of intrinsic defects in the hBN matrix [3,4]. The resulting high-purity crystals have released the engineering potential of this material for the development of efficient light-emitting devices in deep ultraviolet [5,6]. More recently, hBN has even attracted a renewed interest because it exhibits a two-dimensional (2D) honeycomb structure similar to graphene, which can be used as a building block for the design of complex van der Waals heterostructures [7–10]. Given this wide range of promising applications, it is essential to precisely characterize intrinsic defects hosted in the hBN crystal in order to further optimize the properties of this material. In addition, the possibility to isolate defects at the “single-atom” level would offer new opportunities for applications of 2D materials in quantum technologies [11,12].

In early experiments, the characterization of point defects and stacking faults was mainly realized through ensemble measurements using cathodoluminescence and optical spectroscopy in deep ultraviolet [13–16]. Making use of hBN/graphene heterostructures, it was recently shown that impurities hosted in the hBN matrix can also be detected by measuring local modifications of the conductivity in the graphene layer [17,18]. Using scanning tunneling microscopy (STM), this original approach was even used to isolate and manipulate *individual* defects with nanoscale resolution [18].

In this Rapid Communication, we follow a conceptually simpler strategy to probe individual defects in a high-purity hBN crystal by measuring the photoluminescence (PL) response under optical illumination with an energy much lower than the band gap [19–22]. This method is relatively easy to implement in hBN owing to its very large band gap  $E_g \sim 6$  eV [23]. Here we isolate individual defects emitting around 2 eV with a high photostability under ambient conditions. A detailed analysis of the photophysical properties indicates a highly efficient radiative transition leading to one of the brightest

single photon sources reported to date for a bulk material without integrated photonic structures.

The optical response of a high-purity hBN crystal supplied by HQ Graphene [Fig. 1(a)] was analyzed using a scanning confocal microscope operating under ambient conditions. Optical illumination was carried out at the wavelength

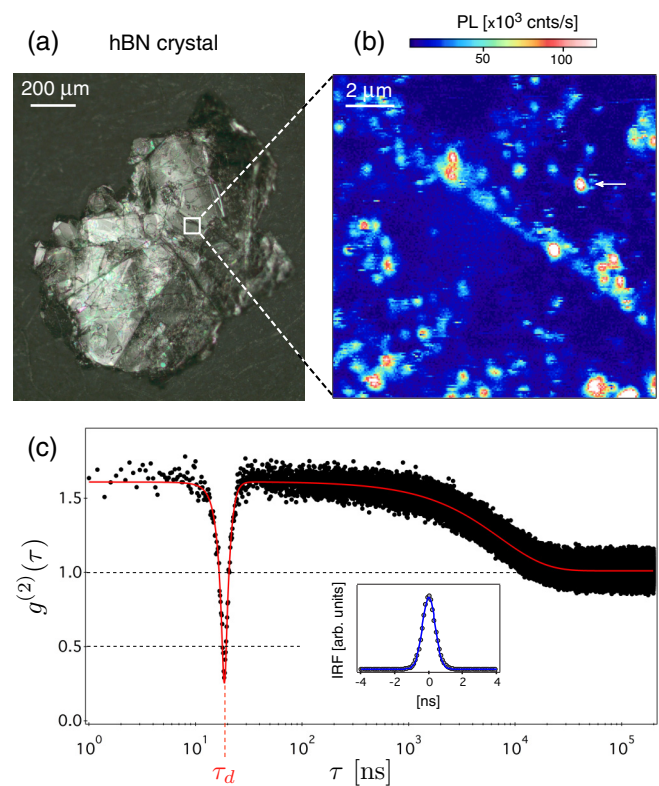


FIG. 1. (a) Microscope image of a high-purity hBN crystal from HQ Graphene. (b) PL raster scan of the sample. (c)  $g^{(2)}(\tau)$  function recorded from the PL spot shown by the white arrow in (b) for a laser excitation power  $\mathcal{P} = 150 \mu\text{W}$  and a bin width  $w = 200$  ps. The solid line is data fitting using a three-level model while including the IRF of the detection setup (see main text). For this experiment we obtain  $\lambda_1 = 0.51 \text{ ns}^{-1}$ ,  $\lambda_2 = 0.14 \mu\text{s}^{-1}$ , and  $a = 0.6$ . Inset: IRF measured using 50-ps laser pulses. The solid line is a Gaussian fit.

\*vincent.jacques@umontpellier.fr

$\lambda = 532$  nm, which allows one to probe deep defects with energy levels far within the band gap of hBN. The excitation laser was focused onto the sample with a high numerical aperture oil-immersion microscope objective (NA = 1.35) mounted on an *xyz*-piezoelectric scanner. The resulting laser spot size on the sample is on the order of  $\sim 300 \times 300$  nm<sup>2</sup>. The PL response of the hBN crystal was collected by the same objective and spectrally filtered from the remaining excitation laser with a razor-edge long-pass filter at 532 nm (Semrock, LP03-532RU). The collected PL was then focused in a 50- $\mu$ m-diameter pinhole and finally directed either to a spectrometer (Ocean Optics, QE Pro-FL) or to silicon avalanche photodiodes operating in the single-photon counting regime (Perkin Elmer, AQR-14). The overall detection efficiency of the experimental setup is on the order of  $\eta_d \sim 1\%$ . A typical PL raster scan of the sample is shown in Fig. 1(b), revealing bright diffraction-limited spots, which correspond to the emission from deep defects hosted in the hBN matrix.

The single-atom nature of the emitters was verified by measuring the second-order correlation function  $g^{(2)}(\tau)$  using two avalanche photodiodes,  $D_1$  and  $D_2$ , mounted in a Hanbury Brown and Twiss (HBT) configuration. Such a detection scheme is commonly used in a “start-stop” mode to record the histogram of time intervals  $K(\tau)$  between two consecutive single-photon detections. Once properly normalized to a Poissonian light source, the recorded histogram is equivalent to the second-order correlation function  $g^{(2)}(\tau)$  provided that  $\tau \ll R^{-1}$ , where  $R$  is the photon detection rate [24,25]. We stress that significant deviations from this equivalence have been experimentally evidenced as soon as  $\tau \gtrsim 100$  ns for  $R \sim 10^5$  s<sup>-1</sup> [26]. The *start-stop* method is thus limited to correlation measurements at very short time scales.

In order to record the  $g^{(2)}(\tau)$  function without any temporal restrictions, the HBT setup was rather used to measure  $J(\tau)$ , defined as the number of photons detected at time  $\tau$  provided that a photon is detected at time  $t = 0$ . To this end, a photon detection event on detector  $D_1$  was used to trigger the acquisition of a PL time trace on detector  $D_2$  using a large-range time-to-digital converter (FastComtec, P7889). After  $\mathcal{N}$  repetitions of the measurement, the resulting time trace  $J(\tau)$  is directly linked to the second-order correlation function through  $g^{(2)}(\tau) = J(\tau)/(\mathcal{N}wR_2)$ , where  $w$  is the bin time and  $R_2$  is the photon detection rate on detector  $D_2$ . Experimentally, an electronic delay  $\tau_d$  was introduced in order to obtain the full profile of the  $g^{(2)}(\tau)$  function at short time scale.

Figure 1(c) shows a typical  $g^{(2)}(\tau)$  measurement recorded over five temporal decades from an isolated PL spot of the hBN crystal. The anticorrelation effect observed at short time scale,  $g^2(\tau_d) \approx 0.25 < 0.5$ , is the signature of single photon emission from an individual defect. The deviation from an ideal anticorrelation [ $g^2(\tau_d) = 0$ ] cannot be explained by a residual background PL from the host matrix owing to the high value of the signal-to-background ratio ( $> 20$ ) [27]. It rather results from the instrumental response function (IRF) of the detection setup, which is mainly fixed by the time jitter of the single-photon detectors [see inset in Fig. 1(c)] [28]. The correlation function also reveals photon bunching  $g^{(2)}(\tau) > 1$ , which indicates that optical cycles involve a nonradiative relaxation path through a long-lived metastable level. Mod-

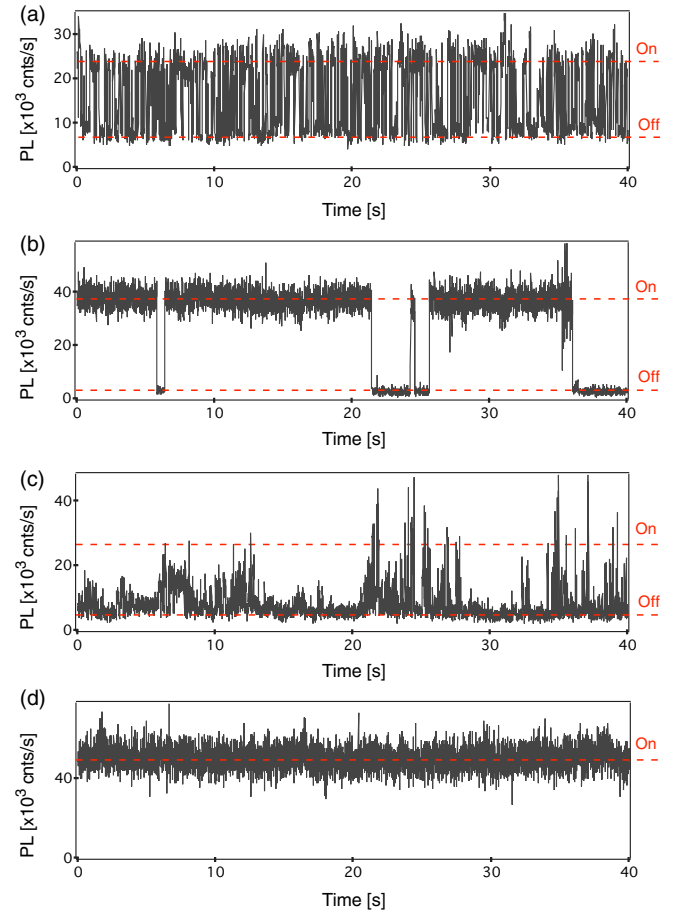


FIG. 2. (a)–(d) Typical PL time traces recorded from different individual defects in a high-purity hBN crystal. The switching rate between the *on* and *off* states varies significantly from one emitter to another. The laser excitation power is set to  $\mathcal{P} = 10$   $\mu$ W. Bin size: 10 ms.

eling the defect as a three-level system [see Fig. 4(a)], the second-order correlation function can be expressed as [29]

$$g^{(2)}(\tau) = 1 - (1 + a)e^{-\lambda_1|\tau-\tau_d|} + ae^{-\lambda_2|\tau-\tau_d|}, \quad (1)$$

where  $a$  is the photon bunching amplitude and  $\lambda_1$  (respectively,  $\lambda_2$ ) is the decay rate of the anticorrelation (respectively, bunching) effect [30]. As shown in Fig. 1(c), the experimental data are well fitted by the convolution of Eq. (1) with the independently measured IRF of the detection setup. A detailed analysis of the dynamics of optical cycles by means of photon correlation measurements is given in the last section of this Rapid Communication.

An important property of any individual defect acting as a single photon source is its photostability over time. Representative PL time traces recorded at low laser power from individual defects hosted in hBN are shown in Fig. 2. Most defects exhibit a pronounced blinking behavior, as often observed for solid-state emitters at room temperature such as quantum dots [31], dye molecules [32], and deep defects in wide-band-gap materials [33–36]. The switching rate between the *on* and *off* states varies significantly from one emitter to another [Figs. 2(a)–2(c)], which suggests that the blinking dynamics are strongly linked to the local environment of the

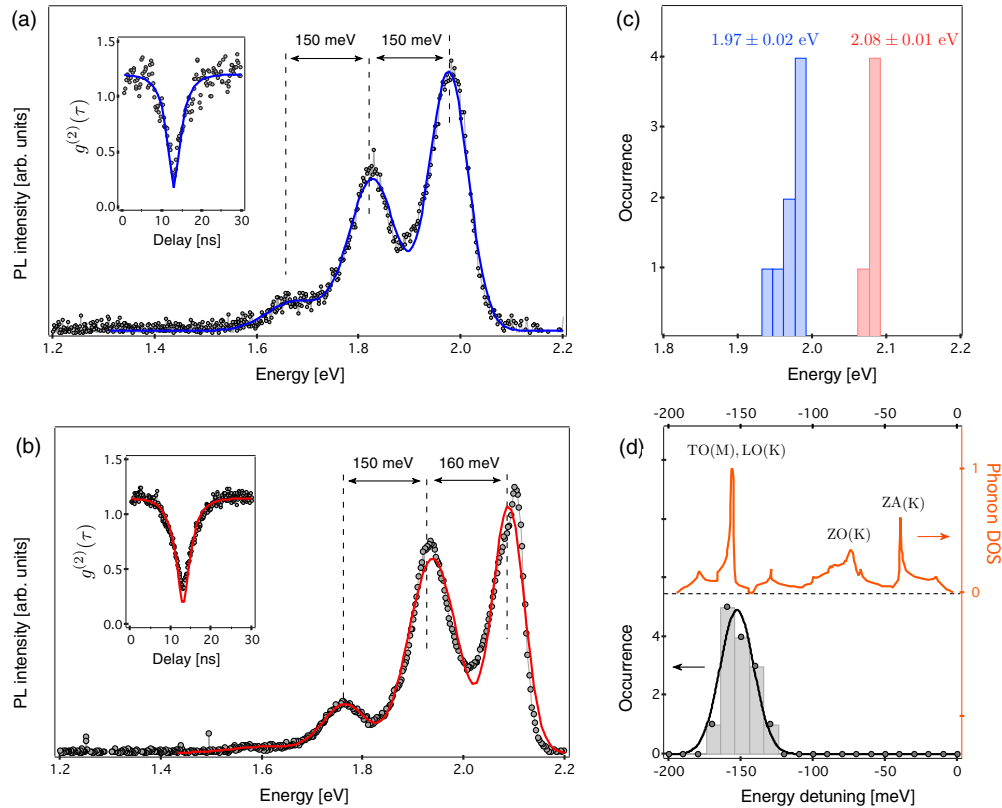


FIG. 3. (a), (b) PL spectra recorded from individual defects in hBN at room temperature under green laser illumination. The solid lines are data fitting with Gaussian functions. The insets show the corresponding second-order correlation function  $g^{(2)}(\tau)$ . The spectrum shown in (a) [respectively, (b)] corresponds to the PL time trace shown Fig. 2(b) [respectively, Fig. 2(d)]. (c) Histogram of the ZPL energy for a set of 13 single defects. Two families of defects can be observed with ZPL energies at  $1.97 \pm 0.02$  eV and  $2.08 \pm 0.01$  eV. (d) Bottom: Histogram of the energy detuning between phonon replica. The solid line is a guide for the eye. Top: phonon density of states (DOS) in hBN extracted from Ref. [39].

defect. Such a blinking could originate from optically induced charge state conversion mediated by a charge exchange with other defects acting as electron donors/acceptors. Permanent photobleaching, i.e., the irreversible conversion of an optically active defect into a nonfluorescent entity, was also observed after a few minutes of optical illumination for most emitters. However, we stress that around 5% of the emitters exhibit a *perfect photostability* over time [Fig. 2(d)], even under high laser excitation power, as observed for a few types of defects in diamond and SiC at room temperature [37,38]. This ratio might be improved through annealing procedures and/or chemical modifications of the sample surface [35,36]. On average, one stable defect could be found in each  $50 \times 50 \mu\text{m}^2$  scan of the sample.

Typical emission spectra recorded at room temperature from individual emitters are shown in Figs. 3(a) and 3(b). We identify two families of spectra with zero-phonon line (ZPL) energies at  $1.97 \pm 0.02$  eV (629 nm) and  $2.08 \pm 0.01$  eV (596 nm) [Fig. 3(c)]. No correlation could be found between the spectrum and the photostability of the defect. The overall structure of the spectra is very similar for the two families, including well-resolved phonon replica with a characteristic energy detuning of  $150 \pm 10$  meV [Fig. 3(d)] between consecutive replicas. A similar energy spacing was recently reported

in the case of single defects in multilayer hBN flakes [19–21]. In fact, this value fairly matches an extremum of the phonon density of states in bulk hBN linked to transverse (TO) and longitudinal (LO) optical phonons at the  $K$  and  $M$  points of the Brillouin zone [Fig. 3(d)] [39]. Our defects being linked to deep levels with a transition energy much smaller than the 6-eV band gap of hBN, we expect an extension of the electronic wave function comparable to, or smaller than the lattice parameter of the hBN matrix [40]. As a consequence, the defect wave function in  $k$  space is spread over the whole Brillouin zone with a significant coupling to the zone-edge phonons, e.g., at the  $K$  and  $M$  points. Since the interaction with optical phonons is much more efficient than with acoustic ones [23], we interpret the systematic 150-meV-energy detuning of the phonon replica as resulting from a dominant coupling to the zone-edge optical phonons of highest density of states [see Fig. 3(d)].

Individual defects in wide-band-gap materials can often be found in various charge states having very different optical properties. A well-known example is the nitrogen-vacancy (NV) defect in diamond, whose ZPL energy is shifted by  $\approx 200$  meV depending on the charge state  $\text{NV}^0/\text{NV}^-$  of the defect [41,42], and becomes even optically inactive in its positively charged state  $\text{NV}^+$  [43,44]. Using a STM, it was

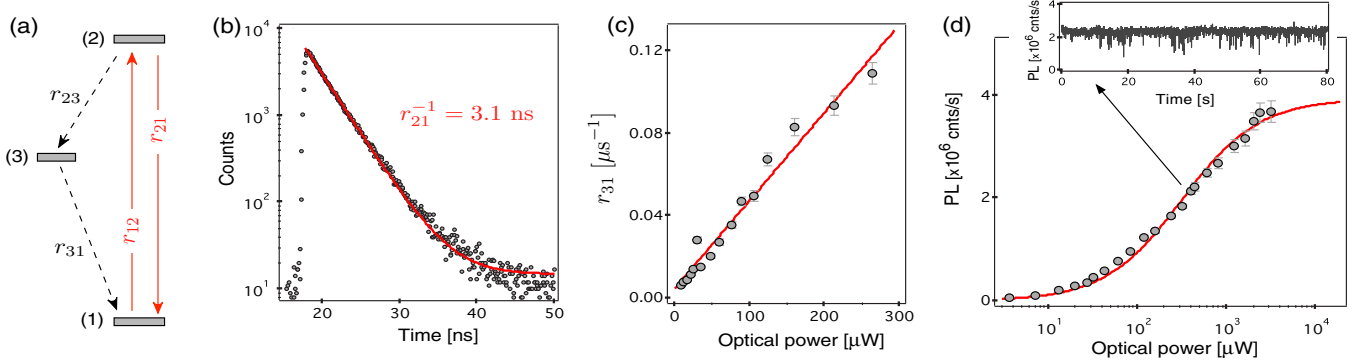


FIG. 4. (a) Three-level model including a radiative transition between the ground (1) and excited (2) levels, and a nonradiative decay through a metastable level (3). The coefficient  $r_{ij}$  denotes the transition rate from level ( $i$ ) to level ( $j$ ). (b) PL decay recorded under optical excitation with 50-ps laser pulses. The solid line is data fitting with a single exponential function. (c) Decay rate of the metastable state  $r_{31}$  as a function of the laser excitation power. The solid line is data fitting with a linear function (see main text). (d) PL saturation curve of the defect. The red solid line is data fitting with a saturation function (see main text). The inset shows a PL time trace recorded for a laser excitation power  $\mathcal{P} = 400 \mu\text{W}$ . We note that short blinking events start to be observed for such laser power above the saturation of the transition. All these measurements are performed on the same individual defect.

recently shown that individual defects in hBN can also be found in positive, negative, and neutral charge states. Active charge state manipulation was even demonstrated by tuning the Fermi energy level with respect to the defect's charge transition level by locally applying an electric field with a STM tip [18]. We tentatively attribute the two groups of spectra shown in Fig. 3 to different charge states of the same defect, while the small variation of the ZPL energy in each group ( $\pm 20$  meV) might result from variations of the strain in the hBN matrix. Optically induced charge state conversion towards a dark state might also play an important role in the blinking/bleaching dynamics of the defect.

We now investigate the dynamics of optical cycles for a stable defect showing a PL spectrum similar to the one shown in Fig. 3(b). The defect is modeled as a three-level system [Fig. 4(a)]. The lifetime of the excited level was first measured through time-resolved PL measurements using a pulsed laser excitation with a 50-ps pulse duration and a 10-MHz repetition rate (PicoQuant, LDH-P-FA-530B). As shown in Fig. 4(b), the PL decay is well fitted by a single exponential function, leading to a lifetime of the excited level  $r_{21}^{-1} = 3.1 \pm 0.1$  ns. This value is in good agreement with the ones recently measured in hBN flakes for individual defects showing similar spectral properties [19,20]. To gain insights into the dynamics of the metastable level, the characteristic parameters of the bunching effect ( $a, \lambda_2$ ) were inferred from  $g^{(2)}(\tau)$  measurements recorded at different laser excitation powers  $\mathcal{P}$  [see Eq. (1)]. Using a three-level model, the relaxation rate of the metastable level  $r_{31}$  is then simply given by [29]

$$r_{31} = \frac{\lambda_2}{1+a}. \quad (2)$$

As shown in Fig. 4(c), our results indicate a pronounced increase in  $r_{31}$  with the laser power, which suggests that optical illumination induces deshelling of the metastable level. This effect, which is often observed for individual emitters in solid-state systems, can be modeled by a

linear power dependence of the deshelling process  $r_{31} = r_{31}^0(1 + \beta\mathcal{P})$  [26,28]. By fitting the data with this equation, we obtain an estimate of the metastable level lifetime  $[r_{31}^0]^{-1} = 210 \pm 80 \mu\text{s}$  and  $\beta = 0.09 \pm 0.04 \mu\text{W}^{-1}$ .

The PL rate  $R$  was finally measured as a function of  $\mathcal{P}$  [Fig. 4(d)]. Data fitting with a simple saturation function  $R = R_\infty/(1 + \mathcal{P}/\mathcal{P}_{\text{sat}})$  leads to a saturation power  $\mathcal{P}_{\text{sat}} = 310 \pm 20 \mu\text{W}$  and an emission rate at saturation  $R_\infty = 3.9 \pm 0.1 \times 10^6$  counts  $\text{s}^{-1}$ , corresponding to one of the brightest single photon sources reported to date. For comparison, the emission rate at saturation is  $\sim 20$  times larger than the one obtained from a single NV defect in diamond with the same confocal microscope. Such high counting rates indicate that the short excited-level lifetime results from a strong radiative oscillator strength with near-unit quantum efficiency rather than PL quenching involving fast nonradiative decay processes ( $r_{23} \ll r_{21}$ ).

To summarize, we have isolated individual defects in a commercial high-purity hBN crystal, leading to a robust single photon source with up to  $\sim 4 \times 10^6$  counts  $\text{s}^{-1}$  under ambient conditions. The analysis of the photophysical properties of the defect provides important information for understanding its structure using *ab initio* calculations [45]. These results pave the road towards applications of hBN, and more generally van der Waals heterostructures, in photonic-based quantum information science [46] and optoelectronics [17].

We thank M. Kociak, A. Zobelli, J.-F. Roch, and I. Robert-Philip for fruitful discussions. This work was financially supported by the network GaNeX (ANR-11-LABX-0014). GaNeX belongs to the publicly funded *Investissement d'Avenir* program managed by the French ANR agency. The authors acknowledge support from Ecole Normale Supérieure de Cachan, Conicyt-Fondecyt (Grant No. 1141185), Conicyt-PCHA Doctoral program (Grant No. 2013-21130747), and PMI PUC 1203.

- [1] R. T. Paine and C. K. Narula, *Chem. Rev.* **90**, 73 (1990).
- [2] X. F. Jiang, Q. H. Weng, X. B. Wang, X. Li, J. Zhang, D. Golberg, and Y. Bando, *J. Mater. Sci. Technol.* **31**, 589 (2015).
- [3] K. Watanabe, T. Taniguchi, and H. Kanda, *Nat. Mater.* **3**, 404 (2004).
- [4] T. Taniguchi and K. Watanabe, *J. Cryst. Growth* **303**, 525 (2007).
- [5] Y. Kubota, K. Watanabe, O. Tsuda, and T. Taniguchi, *Science* **317**, 932 (2007).
- [6] K. Watanabe, T. Taniguchi, T. Niiyama, K. Miya, and M. Taniguchi, *Nat. Photon.* **3**, 591 (2009).
- [7] C. R. Dean *et al.*, *Nat. Nanotechnol.* **5**, 722 (2010).
- [8] A. K. Geim and I. V. Grigorieva, *Nature (London)* **499**, 419 (2013).
- [9] X. Cui *et al.*, *Nat. Nanotechnol.* **10**, 534 (2015).
- [10] F. Withers *et al.*, *Nat. Mater.* **14**, 301 (2015).
- [11] D. D. Awschalom, L. C. Bassett, A. S. Dzurak, E. L. Hu, and J. R. Petta, *Science* **339**, 1174 (2013).
- [12] W. F. Koehla, H. Seo, G. Gallia, and D. D. Awschalom, *MRS Bull.* **40**, 1146 (2015).
- [13] M. G. Silly, P. Jaffrennou, J. Barjon, J.-S. Lauret, F. Ducastelle, A. Loiseau, E. Obraztsova, B. Attal-Tretout, and E. Rosencher, *Phys. Rev. B* **75**, 085205 (2007).
- [14] L. Miseur, E. Feldbach, and A. Kanaev, *Phys. Rev. B* **78**, 155204 (2008).
- [15] R. Bourrellier *et al.*, *ACS Photon.* **1**, 857 (2014).
- [16] G. Cassaboïs, P. Valvin, and B. Gil, *Phys. Rev. B* **93**, 035207 (2016).
- [17] L. Ju *et al.*, *Nat. Nanotechnol.* **9**, 348 (2014).
- [18] D. Wong *et al.*, *Nat. Nanotechnol.* **10**, 949 (2015).
- [19] T. T. Tran, K. Bray, M. J. Ford, M. Toth, and I. Aharonovich, *Nat. Nanotechnol.* **11**, 37 (2016).
- [20] T. T. Tran, C. Elbadawi, D. Totonjian, C. J. Lobo, G. Grosso, H. Moon, D. R. Englund, M. J. Ford, I. Aharonovich, and M. Toth, *ACS Nano* **10**, 7331 (2016).
- [21] N. R. Jungwirth, B. Calderon, Y. Ji, M. G. Spencer, M. E. Flatté, and G. D. Fuchs, *Nano Lett.*, doi:10.1021/acs.nanolett.6b01987.
- [22] T. T. Tran, C. Zachreson, A. M. Berhane, K. Bray, R. G. Sandstrom, L. H. Li, T. Taniguchi, K. Watanabe, I. Aharonovich, and M. Toth, *Phys. Rev. Appl.* **5**, 034005 (2016).
- [23] G. Cassaboïs, P. Valvin, and B. Gil, *Nat. Photon.* **10**, 262 (2016).
- [24] S. Reynaud, *Ann. Phys. (Paris, Fr.)* **8**, 315 (1983).
- [25] C.-H. Huang, Y.-H. Wen, and Y.-W. Liu, *Opt. Express* **24**, 4278 (2016).
- [26] L. Fleury, J.-M. Segura, G. Zumofen, B. Hecht, and U. P. Wild, *Phys. Rev. Lett.* **84**, 1148 (2000).
- [27] A. Beveratos, A. S. Köhn, R. Brouri, T. Gacoin, J. P. Poizat, and P. Grangier, *Eur. Phys. J. D* **18**, 191 (2002).
- [28] E. Wu, V. Jacques, H. Zeng, P. Grangier, F. Treussart, and J.-F. Roch, *Opt. Express* **14**, 1296 (2006).
- [29] S. C. Kitson, P. Jonsson, J. G. Rarity, and P. R. Tapster, *Phys. Rev. A* **58**, 620 (1998).
- [30] This expression is valid if  $(r_{23}, r_{31}) \ll r_{21}$ .
- [31] M. Nirmal, B. O. Dabbousi, M. G. Bawendi, J. J. Macklin, J. K. Trautman, T. D. Harris, and L. E. Brus, *Nature (London)* **383**, 802 (1996).
- [32] R. M. Dickson, A. B. Cubitt, R. Y. Tsien, and W. E. Moerner, *Nature (London)* **388**, 355 (1997).
- [33] S. Choi, B. C. Johnson, S. Castelletto, C. Ton-That, M. R. Phillips, and I. Aharonovich, *Appl. Phys. Lett.* **104**, 261101 (2014).
- [34] A. J. Morfa, B. C. Gibson, M. Karg, T. J. Karle, A. D. Greentree, P. Mulvaney, and S. Tomljenovic-Hanic, *Nano Lett.* **12**, 949 (2012).
- [35] C. Bradac *et al.*, *Nat. Nanotechnol.* **5**, 345 (2010).
- [36] S. Castelletto, B. C. Johnson, V. Ivády, N. Stavrias, T. Umeda, A. Gali, and T. Ohshima, *Nat. Mater.* **13**, 151 (2014).
- [37] I. Aharonovich, S. Castelletto, D. A. Simpson, C.-H. Su, A. D. Greentree, and S. Praver, *Rep. Prog. Phys.* **74**, 076501 (2011).
- [38] B. Lienhard, T. Schröder, S. Mouradian, F. Dolde, T. T. Tran, I. Aharonovich, and D. Englund, *Optica* **3**, 768 (2016).
- [39] G. Kern, G. Kresse, and J. Hafner, *Phys. Rev. B* **59**, 8551 (1999).
- [40] M. Jaros and S. F. Ross, *J. Phys. C: Solid State Phys.* **6**, 1753 (1973).
- [41] L. Rondin, G. Dantelle, A. Slablab, F. Grosshans, F. Treussart, P. Bergonzo, S. Perruchas, T. Gacoin, M. Chaigneau, H.-C. Chang, V. Jacques, and J.-F. Roch, *Phys. Rev. B* **82**, 115449 (2010).
- [42] M. V. Hauf, B. Grotz, B. Naydenov, M. Dankerl, S. Pezzagna, J. Meijer, F. Jelezko, J. Wrachtrup, M. Stutzmann, F. Reinhard, and J. A. Garrido, *Phys. Rev. B* **83**, 081304 (2011).
- [43] B. Grotz *et al.*, *Nat. Commun.* **3**, 729 (2012).
- [44] C. Schreyvogel, V. Polyakov, R. Wunderlich, J. Meijer, and C. E. Nebel, *Sci. Rep.* **5**, 12160 (2015).
- [45] C. Attacalite, M. Bockstedte, A. Marini, A. Rubio, and L. Wirtz, *Phys. Rev. B* **83**, 144115 (2011).
- [46] J. L. O'Brien, A. Furusawa, and J. Vucković, *Nat. Photon.* **3**, 687 (2009).